

Modeling apparent Pb loss in zircon U–Pb geochronology

Glenn R. Sharman¹, Matthew A. Malkowski²

¹Department of Geosciences, University of Arkansas, Fayetteville, AR 72701, USA

²Department of Earth and Planetary Sciences, Jackson School of Geosciences, University of Texas at Austin, Austin, TX 78712, USA

Correspondence to: Glenn R. Sharman (gsharman@uark.edu)

Abstract. The loss of radiogenic Pb from zircon is known to be a major factor that can cause inaccuracy in the U–Pb geochronological system, hence there is a need to better characterize the distribution of Pb loss in natural samples. Treatment of zircon by chemical abrasion (CA) has become standard practice in isotope dilution-thermal ionization mass spectrometry (ID-TIMS), but CA is much less commonly employed prior to *in-situ* analysis via laser ablation-inductively coupled plasma-mass spectrometry (LA-ICP-MS) or secondary ionization mass spectrometry (SIMS). Differentiating the effects of low levels of Pb loss in Phanerozoic zircon with relatively low precision *in-situ* U–Pb dates, where the degree of Pb loss is insufficient to cause discernible discordance, is challenging. We show that U–Pb isotopic ratios that have been perturbed by Pb loss may be modeled by convolving a Gaussian distribution that represents random variations from the true isotopic value stemming from analytical uncertainty with a distribution that characterizes Pb loss. We apply this mathematical framework to model the distribution of apparent Pb loss in 10 igneous samples that have both non-CA LA-ICP-MS or SIMS U–Pb dates and an estimate of the crystallization age, either through CA U–Pb or ⁴⁰Ar/³⁹Ar geochronology. All but one sample showed negative age offsets that were unlikely to have been drawn from an unperturbed U–Pb date distribution. Modeling apparent Pb loss using the logit-normal distribution produced good fits with all 10 samples and showed two contrasting patterns in apparent Pb loss: samples where most zircon U–Pb dates undergo a bulk shift and samples where most zircon U–Pb dates exhibited low age offset but fewer dates had more significant offset. Our modeling framework allows comparison of relative degrees of apparent Pb loss between samples of different age, with the first and second Wasserstein distances providing useful estimates of the total magnitude of apparent Pb loss. Given that the large majority of *in-situ* U–Pb dates are acquired without the CA treatment, this study highlights a pressing need for improved characterization of apparent Pb loss distributions in natural samples to aid in interpreting non-CA *in-situ* U–Pb data and to guide future data collection strategies.

1 Introduction

Zircon U–Pb geochronology is arguably one of the most important radiometric dating approaches used by geoscientists, with widespread application to constraining the age of Pleistocene and older geologic materials (Davis et al., 2003; Schoene, 2013; Gehrels, 2014). We rely on zircon U–Pb dates for calibrating the geological time scale (e.g., Compston, 2000a; 2000b; Bowring

30 and Schmitz, 2003; Gradstein et al., 2004; Kaufmann, 2006), constraining the timing of important Earth history events (Froude
 31 et al., 1983; Burgess et al., 2014), and determining the rates of Earth processes (Rioux et al., 2012; Johnstone et al., 2019). The
 32 zircon U–Pb geochronometer is particularly powerful due to the ability to assess agreement between the $^{238}\text{U} \rightarrow ^{206}\text{Pb}$ and
 33 $^{235}\text{U} \rightarrow ^{207}\text{Pb}$ decay chains, with $^{206}\text{Pb}^*/^{238}\text{U}$ and $^{207}\text{Pb}^*/^{235}\text{U}$ dates in agreement plotting on the Concordia line, where * indicates
 34 radiogenic Pb (Wetherill, 1956).

35

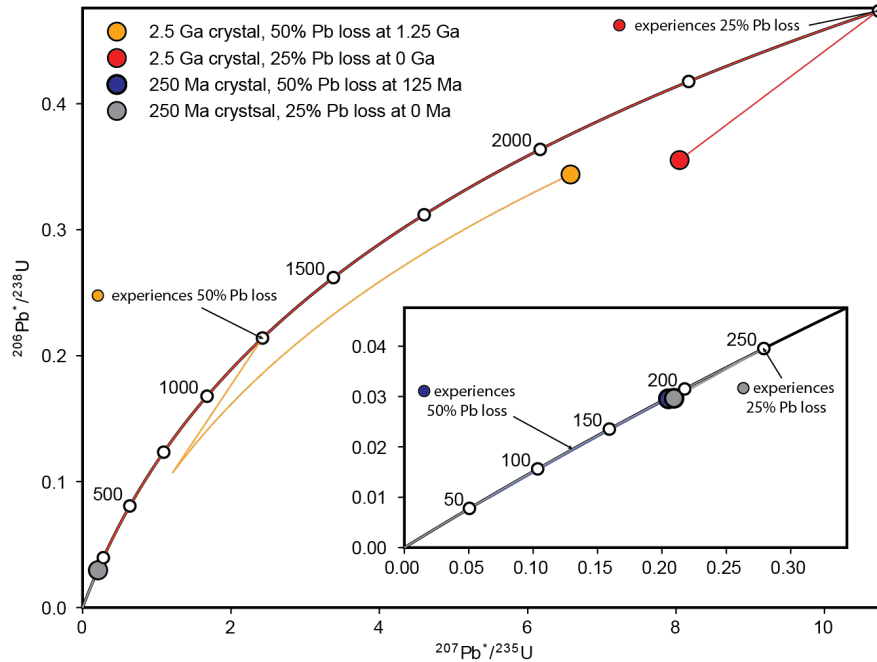


Figure 1. Illustration of the influence of Pb loss on 250 Ma and 2.5 Ga zircon. Two Pb loss scenarios are shown: 25% loss at half the age of the zircon and 50% loss at present-day (0 Ma). The approximately linear nature of the $^{206}\text{Pb}^*/^{238}\text{U}$ vs $^{207}\text{Pb}^*/^{235}\text{U}$ Concordia line near the origin results in Pb loss producing limited discordance if the Pb loss occurs within several 100s of Myr of crystallization. Note that a greater amount of ancient Pb loss is required to produce the same shift in $^{206}\text{Pb}^*/^{238}\text{U}$ relative to recent Pb loss. Thin, colored lines represent the path of each zircon.

36

37

38 The causes and complications of open system behavior (e.g., radiogenic Pb loss) in zircon have long been a topic of study
 39 (Tilton et al., 1955; Pidgeon et al., 1966). Although Pb loss events may be discerned on U–Pb Concordia diagrams in some
 40 circumstances and can provide useful geologic information about the thermal and/or fluid flow history of a region (Silver and
 41 Deutsch, 1963; Blackburn et al., 2011; Morris et al., 2015; Kirkland et al., 2017), recognizing Pb loss remains a challenge
 42 when it occurs within several 100’s Myr of crystallization (Fig. 1; Anderson et al., 2019). For example, due to the shape of the
 43 $^{206}\text{Pb}^*/^{238}\text{U}$ versus $^{207}\text{Pb}^*/^{235}\text{U}$ Concordia line, Pb loss in Phanerozoic zircon results in a ‘sliding along concordia’ effect that

44 can make Pb loss difficult to discern, particularly in relatively low-precision *in-situ* (i.e., LA-ICP-MS or SIMS) datasets when
45 the Pb loss produces concordant or only modestly discordant analyses (e.g., <10%; Ashwal et al., 1999; Bowring and Schmitz,
46 2003; Ireland and Williams, 2003; Reimink et al., 2016; Spencer et al., 2016; Watts et al., 2016; Anderson et al., 2019). Such
47 low levels of Pb loss have been termed ‘cryptic’ and may be associated with spatial heterogeneities including radiation-
48 damaged U-rich zones and microstructures (Nasdala et al., 2005; Kryza et al., 2012; Watts et al., 2016). Although there are
49 many potential causes of Pb loss in zircon, open system behavior is often associated with elevated α -dose and associated
50 metamictization (Silver and Deutsch, 1963; Pidgeon et al., 1966; Mezger and Krogstad, 1997; Cherniak and Watson, 2001;
51 Marsellos and Garver, 2010). Mechanisms for Pb loss include recrystallization of metamict zircon during metamorphism
52 (Kröner et al., 1994; Mezger and Krogstad, 1997; Orejana et al., 2015; Zeh et al., 2016) and leaching of Pb from metamict
53 zones by hydrothermal or diagenetic fluids (Geisler et al., 2002, 2003; Willner et al., 2003; Morris et al., 2015; Kirkland et al.,
54 2020) or during chemical weathering (Stern et al., 1966; Black, 1987; Balan et al., 2001; Pidgeon et al., 2017; Andersen and
55 Elburg, 2022). Pb loss is thought to primarily occur at temperatures <250°C in which radiation damage in zircon is unable to
56 be annealed over geologic timescales (Schoene, 2013).

57
58 Zircon domains that have lost Pb may be preferentially removed by first thermally annealing the zircon at high temperature
59 (e.g., 800-1100°C) and then partially dissolving the zircon in a heated HF solution in a technique called chemical abrasion
60 (CA) (Mattinson, 2005). The CA treatment is now routinely applied in ID-TIMS analysis and has contributed to both improved
61 precision and accuracy of CA-ID-TIMS U–Pb data (Schoene, 2013). Although some *in-situ* U–Pb laboratories practice thermal
62 annealing routinely (e.g., Allen and Campbell, 2012; Solari et al., 2015), CA has been applied much less frequently (Crowley
63 et al., 2014; von Quadt et al., 2014; Watts et al., 2016; Ver Hoeve et al., 2018; Ruiz et al., 2022). Several studies that have
64 conducted paired analysis of non-CA and CA of the same samples via *in-situ* U–Pb geochronology have found the non-CA
65 U–Pb dates to skew younger than the CA U–Pb dates (Crowley et al., 2014; von Quadt et al., 2014; Watts et al., 2016). A
66 growing number of maximum depositional age studies with tandem non-CA LA-ICP-MS and CA-ID-TIMS dating have shown
67 the youngest non-CA U–Pb dates tend to be younger than expected relative to CA U–Pb dates or other geologic constraints,
68 even when considering measurement uncertainty (e.g., Herriott et al., 2019; Schwartz et al., 2022; Howard et al., 2022;
69 Sharman et al., 2023). However, there is a lack of quantitative constraints on the relative importance of Pb loss in influencing
70 non-CA U–Pb date distributions acquired via *in-situ* mass spectrometry, particularly as related to influencing depositional age
71 constraints (Copeland, 2020).

72
73 This study builds upon past research on open system behavior in zircon by presenting a mathematical framework for
74 characterizing the distribution of apparent Pb loss on untreated (i.e., non-CA) U–Pb date distributions. We first suggest that
75 U–Pb isotopic ratios that have been perturbed by Pb loss may be viewed as the convolution of two signals: a Gaussian
76 distribution that reflects measurement uncertainty about the true isotopic ratio and the distribution that characterizes Pb loss.
77 We then apply this mathematical framework to model the distribution of apparent Pb loss that has affected 10 igneous samples

78 of Miocene to Carboniferous age. Our results highlight the importance of quantifying distributions of apparent Pb loss
 79 magnitude to better understand the potential influence on non-CA zircon U–Pb date distributions.
 80

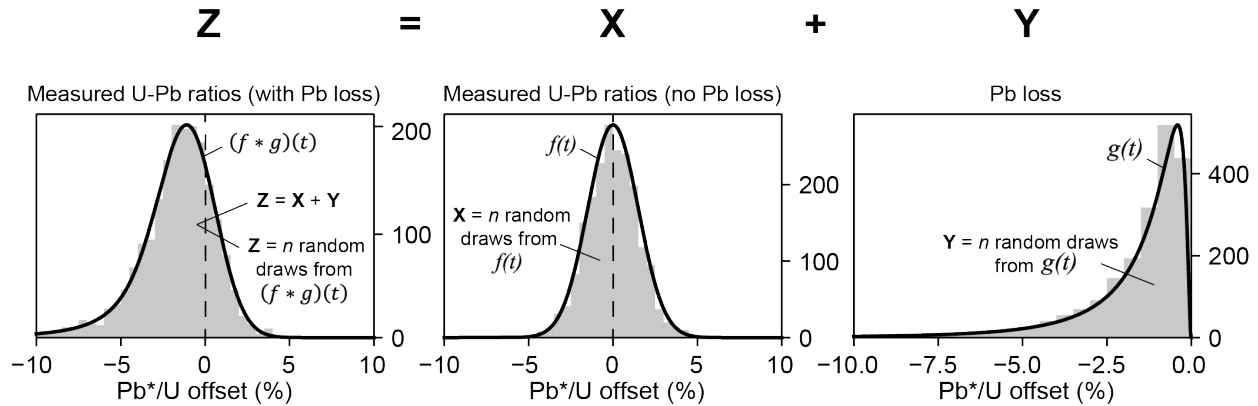


Figure 2. Illustration of how Pb*/U isotopic ratios from n zircon analyses that have been perturbed by Pb loss (Z) may be modeled as the summation of n non-perturbed Pb*/U ratios (X) and the amount of Pb loss encountered by each (Y). X is drawn from $f(t)$ that reflects the Gaussian distribution of Pb*/U ratios that are unperturbed by Pb loss and Y is drawn from $g(t)$ that represents the distribution of Pb loss in the sample. The distribution that characterizes Z may be found by convolving $f(t)$ and $g(t)$. Although we assume that $f(t)$ is a Gaussian distribution, the distribution type of Pb loss, $g(t)$, shown in this example as a logit-normal distribution ($\mu=-4.5$, $\sigma=1.0$) could take a number of discrete or continuous forms (Fig. 3). Note that in our modeling framework, values of X , Y , and Z are normalized as percentage deviation from the true isotopic ratio (i.e., the mean of $f(t)$), where negative values indicate that measured Pb*/U is lower than the true ratio. See Supplemental Video 1 for an animation that illustrates the process of convolution and Supplemental Video 2 for an exploration of the logit-normal distribution in μ and σ parameter space.

81 2 Mathematical framework

82 A series of n Pb*/U measurements that have undergone Pb loss, Z , may be modeled as the sum of the corresponding
 83 unperturbed Pb*/U values, X , and the amount that Pb*/U changed due to Pb loss for each date, Y ,

$$84 \quad Z = X + Y \quad (\text{Equation 1})$$

85 where Z , X , and Y are all 1-D matrices with n values and units of percentage offset from the true isotopic value (Fig. 2).
 86 Because Pb loss produces a lower Pb*/U ratio, the values of Y must be negative in our formulation of Equation 1. If X is drawn
 87 from a Gaussian distribution $f(t)$ whose mean (μ) approximates the true isotopic value and whose standard deviation (σ) reflects
 88 dispersion from the true value related to measurement uncertainty (e.g., Schoene, 2013) and if Y is drawn from a distribution
 89 that reflects Pb loss, $g(t)$, then Z may be viewed as being drawn from the convolution of $f(t)$ and $g(t)$

$$90 \quad (f * g)(t) = \int_{-\infty}^{\infty} f(\tau)g(t - \tau)d\tau \quad (\text{Equation 2})$$

91 provided that X and Y are independent (Fig. 2; Supplemental Video 1). Convolution simply represents the summation of two
 92 random variables, in this case one related to analytical precision (i.e., random variation around the true isotopic value stemming
 93 from the measurement process) and the other related to the geologic process of Pb loss. We model Pb loss as percentage offset

94 from the true Pb^*/U value rather than deviation in absolute time (i.e., Myr) to promote comparison of samples of different age
 95 (Fig. 2).

96

97 Equation 2 may be solved analytically for some forms of $f(t)$ and $g(t)$. For example, the convolution of Gaussian and
 98 exponential distributions is known as the exponentially modified Gaussian distribution (Grushka, 1972). However,
 99 $(f * g)(t)$ may also be solved numerically, which has the advantage of allowing both $f(t)$ and $g(t)$ to take any form.

100

101

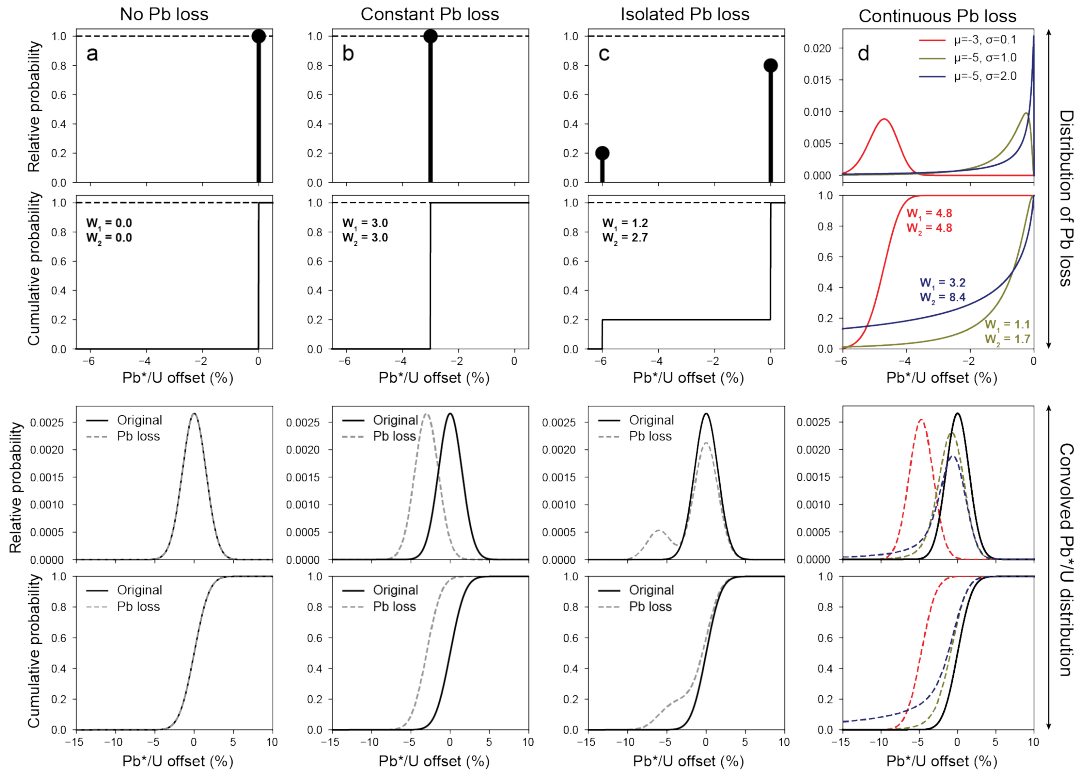


Figure 3. Illustration of how normally distributed zircon Pb^*/U values may be perturbed by discrete (a-c) or continuous (d) distributions of Pb loss. The top row represents the distribution of Pb loss in the sample expressed as a percentage of the true isotopic ratio (e.g., $^{206}Pb^*/^{238}U$ or $^{207}Pb^*/^{235}U$) at the time of Pb loss, where the height of the black bar and ball indicates the relative probability of the specified Pb^*/U offset. Three discrete scenarios are shown: a) no Pb loss, b) constant Pb loss, and c) isolated Pb loss. A logit-normal distribution is shown as an example of continuous Pb loss in d). Additional examples of continuous Pb loss distributions are shown in Figure A1. The bottom row shows both the relative (above) and cumulative (below) probabilities of the unperturbed (solid black line) and Pb loss-perturbed (dashed line) Pb^*/U distributions.

102

103 3 Methods

104 3.1 Modeling approach

105 We use the mathematical framework described above to model both the distribution of apparent Pb loss, $g(t)$, experienced by
106 a group of cogenetic crystals and their unperturbed U–Pb date distribution, $f(t)$. Because Pb loss is isotopically indiscriminate,
107 Equation 2 may be equally applied to $^{206}\text{Pb}^*/^{238}\text{U}$ and $^{207}\text{Pb}^*/^{235}\text{U}$. However, we model $^{206}\text{Pb}^*/^{238}\text{U}$ ratios as these have much
108 lower analytical uncertainty for the Carboniferous and younger samples analyzed in this study.

109
110 To model $g(t)$, we allow the μ of $f(t)$ to vary within the 95% confidence interval associated with an independent estimate of
111 the crystallization age. We then estimate both $g(t)$ and σ of $f(t)$ by iteratively solving for the combination of parameters that
112 minimize the misfit between the measured Pb^*/U values and the modeled distribution $(f * g)(t)$ using the Python
113 `scipy.optimize.minimize()` function. We define misfit as the sum of squared residuals between the empirical cumulative
114 distribution function (ECDF) of the measured Pb^*/U values and the cumulative density function (CDF) of the modeled Pb^*/U
115 distribution.

116
117 If both non-CA and CA analyses are available from the same sample, then the distribution of CA U–Pb dates may be used to
118 constrain the parameters of $f(t)$. For such samples, we modify the approach described above by first finding the Gaussian
119 distribution $f(t)$ that most closely approximates the treated Pb^*/U distribution. We then use this best-fitting $f(t)$ in estimating
120 $g(t)$ using the minimization-of-misfit technique described above. Such datasets have the advantage of providing constraints on
121 σ of $f(t)$, which is otherwise treated as an unknown parameter during modeling if only non-CA U–Pb dates are available.

122
123 In order to estimate $g(t)$ as described above, we must choose one or more reasonable parametric models that are appropriate
124 for describing distributions of Pb loss. One possibility is that all zircon crystals in the sample experienced the same amount of
125 Pb loss, which could shift Pb^*/U from 0% to -100% of its value. Such a scenario of constant Pb loss may be modeled by a
126 discrete form of $g(t)$ where a single parameter specifies the percentage of Pb lost. Convolution of such a discrete form of $g(t)$
127 simply produces a negative shift in the Pb^*/U values (i.e., Fig. 3b).

128
129 Another possibility is that Pb loss was experienced by only a subset of crystals (i.e., isolated Pb loss). This scenario may also
130 be modeled by assigning $g(t)$ to a discrete distribution with two parameters: one that indicates the fraction of Pb lost and one
131 that specifies the proportion of crystals that underwent Pb loss (Fig. 3c). This parameterization of $g(t)$ will produce a bimodal
132 pattern in U–Pb values, particularly if the degree of Pb loss is significant relative to measurement uncertainty (Fig. 3c).

133
134 Instead of modeling $g(t)$ as a discrete distribution where Pb loss is restricted to certain values, we may also consider a
135 continuous probability distribution where values of Pb loss can take on any value between 0% and 100% (Fig. 3d). Rather than

136 assume *a priori* the form(s) that $g(t)$ might take, we considered a wide range of 1- or 2-parameter distributions for the purposes
 137 of exploratory modeling (Appendix A). Of the distribution types considered, we identified the logit-normal distribution, also
 138 known as the logistic normal distribution, as perhaps the most reasonable for modeling Pb loss. The logit-normal distribution
 139 has the property of having a logit (i.e., the quantile function of the logistic distribution) that is normally distributed with a
 140 geometric mean of μ and standard deviation of σ (Aitchison and Shen, 1980; Mead, 1965)

$$141 \quad f(x, \mu, \sigma) = \frac{1}{\sigma\sqrt{2\pi}} \frac{1}{x(1-x)} e^{-\frac{(\text{logit}(x)-\mu)^2}{2\sigma^2}} \quad (\text{Equation 3})$$

142 for $0 < x < 1$. The logit-normal distribution is well-suited for modeling constrained data types (e.g., compositional data; Aitchison
 143 and Bacon-Shone, 1999; Vermeesch, 2018b) in part due to it being defined
 144 over $0 < x < 1$. We invert and scale the distribution to extend from -
 145 $100\% < x < 0\%$ to match the sign and units of Pb*/U offset due to Pb loss
 146 when expressed as a percentage (Fig. 3d).

147
 148 Figure 4 explores the relationship of the logit-normal distribution to its
 149 two parameters (μ and σ) (see also Supplemental Video 2). The
 150 distribution has a ‘spikey’ character when σ is a very small number (e.g.,
 151 0.001; Fig. 4a), which would be a reasonable approximation for samples
 152 that underwent an approximately constant amount of Pb loss (e.g., Figs.
 153 3a and 3b). Although the logit-normal distribution cannot model 0% or
 154 100% Pb loss, these values may be approximated by making μ a large
 155 negative or positive number, respectively. A sample where most zircon
 156 exhibit very little Pb loss but with fewer zircon experiencing significant
 157 Pb loss could be produced by $\mu = -4$ and $\sigma = 1.0$ (Fig. 4c). Alternatively,
 158 a sample with a peak probability of Pb*/U offset $< 0\%$ may be modeled
 159 using moderate values of σ (e.g., 0.25-1; Figs. 4b and 4c). The logit-
 160 normal distribution produces bimodal distributions where most probability
 161 is close to 0% and -100% when σ values are high (e.g., $\gg 1$; Fig. 4d).

162 3.2 Samples

163 We apply the mathematical and modeling framework presented above to estimate the distribution of apparent Pb loss in 10
 164 igneous samples that range in age from Carboniferous to Miocene, nine of which have been published previously (Table 1).
 165 Samples CTU, RCP, and SRF are all from upper Eocene rhyolites of the Caetano caldera system of the western United States
 166 (Watts et al., 2016). These samples were split into non-CA and CA aliquots prior to analysis via SIMS (Watts et al., 2016).
 167 We used the error-weighted mean age of the CA U–Pb dates as an estimate of the true crystallization age for each sample, with

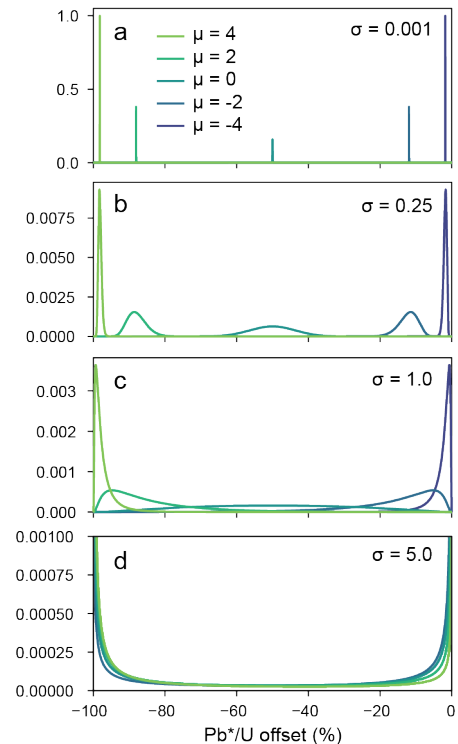


Figure 4. Exploration of the logit-normal distribution's parameter space. Note that we have rescaled the x-axis of the logit-normal distribution such that $-100 < x < 0$.

168 weighted means approximately 0.4-0.6 Myr older than the corresponding $^{40}\text{Ar}/^{39}\text{Ar}$ sanidine ages (Watts et al., 2016). The
 169 number of analyses per aliquot (non-CA or CA) ranges from 17-34 for these three samples (Table 1).
 170

Table 1. Sample Summary

Sample	Age (Ma)	Reference	N (non-CA)	N (CA)	Mean $\log(D_\alpha)^8$	Model results (best fit logit-normal distribution)					
						$f(t)$ (Ma)	$g(t)$ sum of squared residuals	$g(t)$ parameters	$g(t)$ P2.5-P50-P97.5 (%)	W_1	W_2
ELM18 DVTC-10	15.7 ± 0.2 (2 σ) ¹	Miller et al. (2022)	144	n.a.	16.0	15.90 ± 0.55 (1 σ)	1.0	$\mu = -3.24$ $\sigma = 1.28$	-32.49 -3.77 -0.32	6.9	11.1
248-2	24.422 ± 0.25 (2 σ) ³	von Quadt et al. (2014)	30	55	16.8	24.42 ± 0.64 (1 σ)	2.7	$\mu = -4.48$ $\sigma = 1.06$	-8.3 -1.12 -0.14	1.9	3.0
029-5 ⁵	24.480 ± 0.084 (2 σ) ³	von Quadt et al. (2014)	42	48	16.9	24.47 ± 0.79 (1 σ)	3.3	$\mu = -3.10$ $\sigma = 0.47$	-10.17 -4.31 -1.76	4.7	5.2
059-1 ⁵	24.57 ± 0.28 (2 σ) ²	von Quadt et al. (2014)	41	36	17.0	24.50 ± 0.95 (1 σ)	1.1	$\mu = -3.48$ $\sigma = 0.52$	-7.87 -2.99 -1.1	3.4	3.8
CTU	34.41 ± 0.26 (2 σ) ²	Watts et al. (2016)	24	18	16.5	34.47 ± 0.83 (1 σ)	2.1	$\mu = -3.21$ $\sigma = 0.29$	-6.65 -3.88 -2.23	4.0	4.2
RCP	34.38 ± 0.32 (2 σ) ²	Watts et al. (2016)	34	18	16.6	34.19 ± 0.75 (1 σ)	3.1	$\mu = -3.96$ $\sigma = 0.80$	-8.38 -1.87 -0.40	2.5	3.3
SRF	34.62 ± 0.37 (2 σ) ²	Watts et al. (2016)	17	17	16.7	34.25 ± 0.75 (1 σ)	5.1	$\mu = -4.57$ $\sigma = 1.08$	-7.92 -1.03 -0.12	1.8	2.9
DG 026	76.41 ± 0.45 (2 σ) ³	von Quadt et al. (2014)	31	34	16.6	76.16 ± 1.42 (1 σ)	3.0	$\mu = -3.74$ $\sigma = 0.56$	-6.65 -2.32 -0.79	2.7	3.1
MM20-EC-109 ⁶	144.50 ± 0.07 (2 σ) ⁴	This study	68	n.a.	17.8	144.43 ± 3.12 (1 σ)	1.6	$\mu = -4.73$ $\sigma = 1.91$	-27.16 -0.87 -0.02	3.6	8.8
AvQ 244 ⁷	333.60 ± 0.66 (2 σ) ³	von Quadt et al. (2014)	17	19	17.0	333.64 ± 10.86 (1 σ)	12.3	$\mu = -2.69$ $\sigma = 0.82$	-25.30 -6.36 -1.34	8.1	10.3

171
 172 ¹Sanidine $^{39}\text{Ar}/^{40}\text{Ar}$ age (Snow and Lux, 1999)
 173 ²Error-weighted mean of chemically abraded U–Pb dates
 174 ³Concordia age (CA-ID-TIMS)
 175 ⁴Error-weighted mean 5 of 5 zircon crystals analyzed via CA-ID-TIMS
 176 ⁵U–Pb dates older than 28 Ma excluded from analysis
 177 ⁶U–Pb dates older than 158 Ma excluded from analysis
 178 ⁷U–Pb dates older than 360 Ma excluded from analysis
 179 ⁸ D_α is the alpha dose (events g^{-1})
 180 N = Number of analyses
 181 n.a. = Not available
 182 W_1 = first Wasserstein distance
 183 W_2 = second Wasserstein distance

184

185 We present analysis of five samples reported in von Quadt et al. (2014), including upper Oligocene andesite/trachy-andesite
186 from Macedonia (248-2, 029-5, and 059-1), upper Cretaceous dolerite from Romania (DG 026), and middle Carboniferous
187 granite from West-Bulgaria (AvQ 244). These samples were also split into non-CA and CA aliquots prior to analysis via LA-
188 ICP-MS. For samples other than 059-1 we use concordia ages from CA-ID-TIMS analyses of between three and six crystals
189 for the crystallization age of each sample (von Quadt et al., 2014; Table 1). For sample 059-1 we used the weighted mean of
190 the CA U–Pb dates. The number of analyses per sample (non-CA or CA) ranged from 17-55 for this dataset (Table 1).

191

192 Sample ELM18DVTC-10 is from a Miocene ash-flow tuff from the Pangua Formation in the western United States that has
193 144 U–Pb dates acquired via LA-ICP-MS (Miller et al., 2022). We use a $^{40}\text{Ar}/^{39}\text{Ar}$ weighted mean age of 15.7 ± 0.2 Ma (2σ)
194 from the same unit as an estimate of the crystallization age of this sample (sample 592-GV1 of Snow and Lux, 1999). Sample
195 ELM18DVTC-10 was highlighted by Schwartz et al. (2022) who noted the youngest zircon U–Pb dates to be much younger
196 than the accepted $^{40}\text{Ar}/^{39}\text{Ar}$ age of this unit. Miller et al. (2022) also noted the presence of these young zircon and suggested
197 that they may be a consequence of surface contamination from units higher in the section.

198

199 Sample MM20-EC-109 is a Lower Cretaceous intermediate ash interbedded within marine carbonaceous mudstone from the
200 Rio Mayer Formation of Argentina with 68 zircon U–Pb dates acquired via LA-ICP-MS (Table A3). Laser ablation spot
201 locations were selected on the rim and/or core of the zircon guided by CL images (Figure A3), with 59 zircon crystals analyzed
202 in total. We use a crystallization age of 144.43 ± 0.07 Ma (2σ) derived from a weighted mean of five zircon crystals analyzed
203 via CA-ID-TIMS at the Boise State University Isotope Geology Laboratory (Table A4). This sample exhibits a large offset
204 between the youngest U–Pb dates acquired via LA-ICP-MS, up to ~60% younger than the CA-ID-TIMS weighted mean.

205 **3.3 Statistical analysis**

206 To evaluate the likelihood that the measured Pb*/U distribution could have been drawn from the modeled $(f * g)(t)$, we apply
207 the nonparametric, 1-sided Kolmogorov-Smirnov (K-S) and Kuiper statistical tests that compare the ECDF with the cumulative
208 CDF of $(f * g)(t)$ (Press, 2007). The Kuiper statistic is relatively more sensitive in differences in the tails of the distributions
209 versus the K-S statistic (Vermeesch, 2018a). We reject the null hypothesis that the non-CA U–Pb dates were drawn from $(f * g)(t)$
210 if the K-S or Kuiper p-value is <0.05 (i.e., 95% confidence level). We thus interpret p-values >0.05 to indicate that the
211 non-CA U–Pb dates could have been plausibly drawn from $(f * g)(t)$ at a 95% confidence level (Press, 2007). However, it
212 should be noted that Saylor and Sundell (2016) found that both K-S and Kuiper p-values more frequently reject the null
213 hypothesis than expected. We thus use p-values as a general guideline to model goodness-of-fit.

214

215 The Wasserstein distance has been recently proposed as a metric for quantifying the dissimilarity between detrital zircon U–
216 Pb age distributions (Lipp and Vermeesch, 2023). We consider the first and second Wasserstein distances, W_1 and W_2 , to be
217 useful approximations for the total degree of negative Pb*/U perturbation that a set of analyses has experienced,

$$218 \quad W_1 = \int_0^1 |M^{-1} - N^{-1}| dt \quad (\text{Equation 3})$$

$$219 \quad W_2 = \sqrt{\int_0^1 |M^{-1} - N^{-1}|^2 dt} \quad (\text{Equation 4})$$

220 where M^{-1} and N^{-1} are the inverses of the CDFs M and N . Because values of Pb loss are restricted to between 0% and 100%,
221 both W_1 and W_2 yield maximum possible values of 100 (i.e., 100% of analyses have -100% Pb*/U offset, or the U–Pb system
222 is completely reset). The W_1 simply equates to the area beneath the cumulative probability distribution of $g(t)$ (e.g., Fig. 3).
223 Because the W_2 distance involves a squaring of the distance between the quantile functions, it imparts a higher cost penalty for
224 the part of the distribution with strongly offset values. For example, the W_1 and W_2 distances are equal for a Pb loss function
225 characterized by constant Pb loss (e.g., 3% Pb loss produces W_1 and W_2 values of 3, Fig. 3b). However, the W_2 distance is
226 often much larger than W_1 for Pb loss distributions with a heavy tail (Fig. 3d). As such, the W_2/W_1 ratio provides an
227 approximation of Pb loss distribution asymmetry, with values of 1 indicating constant Pb loss and values $\gg 1$ indicating highly
228 asymmetric Pb loss.

229 **4 Results**

230 Of the four primary types of Pb loss distributions considered (Fig. 3), the logit-normal distribution yielded the lowest average
231 misfit with a value of 3.5, followed by the isolated Pb loss scenario (average of 4.5) and the constant Pb loss scenario (average
232 of 10.5) (Table A2). The scenario of no Pb loss performed the worst of any scenario that we considered, with an average misfit
233 of 101.3 (Table A2). Correspondingly, both K-S and Kuiper p-values for the no Pb loss

234

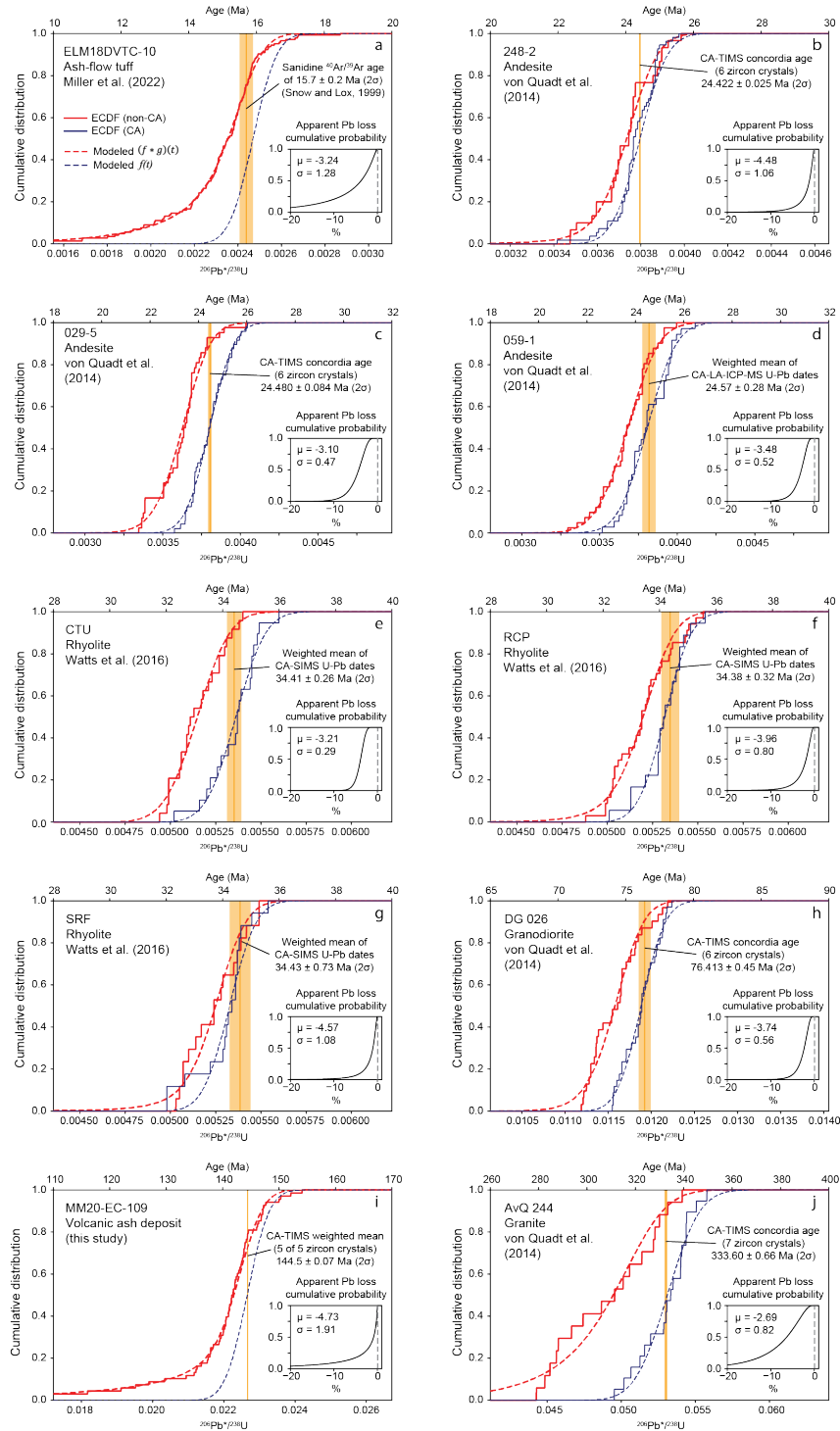


Figure 5. Modeling of apparent Pb loss in zircon U-Pb dates acquired via LA-ICP-MS or SIMS. The best-fitting logit-normal distribution of apparent Pb loss is shown (Table 1; see Figure A1 for plots of all samples and apparent Pb loss distribution types modeled). Empirical cumulative distribution functions (ECDFs) are shown as solid lines while model results are shown as dashed lines. See text for further discussion of model results.

235

236 scenario are $\ll 0.05$ for all samples except SRF, suggesting that the untreated LA-ICP-MS or SIMS U–Pb dates are unlikely
237 to have been drawn from an unperturbed U–Pb date distribution.

238

239 Figure 5 presents a comparison of actual versus modeled U–Pb date distributions for each sample, with the best-fitting logit-
240 normal distribution shown (Table 1; see Figure A1 for individual plots that show the fit for each sample and distribution type).

241 We chose to not consider discrete distributions of $g(t)$ for the “best” fit because we consider it unlikely that Pb loss (or other
242 processes that cause negative age offsets) would be limited to discrete values (e.g., Fig. 3). Values of μ for $g(t)$ ranged from -
243 2.69 to -4.73 with corresponding values of σ spanning 0.29 to 1.91. W_1 distances ranged between 1.8 (sample SRF) and 8.1
244 (sample AvQ 244) and W_2 distances between 2.9 and 11.1 (Table 1; Fig. 5).

245

246 A plot of the best-fitting logit-normal distributions displays two distinct behaviors of $g(t)$ (Fig. 6). (1) Four samples with $\mu <$
247 ~ -3 and $\sigma > 1$ and have a $g(t)$ maximum relative probability close to 0% suggesting a strongly decaying rate of offset (i.e.,
248 most zircon experienced very little Pb loss, while a few have more significant Pb*/U offset). These samples also displayed
249 $W_2/W_1 \geq 1.6$. (2) The remaining six samples that yielded $\sigma < 1$ and generally higher μ values (> -4) displayed a tendency for
250 the mode of $g(t)$ to be $> 0\%$, representing more of a bulk shift in age (e.g., most U–Pb dates have some offset, while relatively
251 few have very little or very much age offset). These samples produced $W_2/W_1 \leq 1.3$.

252 **5 Discussion**

253 **5.1 Assumptions and limitations**

254 The mathematical and modeling framework that we present includes
 255 several underlying assumptions and limitations that should be
 256 considered.

257 1. Because $g(t)$ could represent any geological or analytical
 258 process that introduces negative age offsets, we use the phrase “apparent
 259 Pb loss” when describing our modeled estimates of $g(t)$. For instance,
 260 matrix-related systematic errors (Allen and Campbell, 2012), addition of
 261 U-Th during weathering (Pigeon et al., 2019), and even sample
 262 contamination from younger minerals could introduce negative age shifts
 263 exclusive of loss of radiogenic Pb. Common Pb corrections, particularly
 264 the ^{207}Pb -correction, may also introduce a bias in Pb^*/U values
 265 (Anderson, 2002; Anderson et al., 2019). We recommend that these
 266 additional complexities in the U–Pb system be considered when
 267 interpreting modeled estimates of $g(t)$ as representing distributions of Pb
 268 loss.

270 2. Our approach of parameterizing $g(t)$ for the purpose of
 271 exploratory modeling has the advantage of yielding results that are
 272 interpretable while also being suitable for the relatively low- n datasets
 273 available. However, any parametric model is likely a simplification of the
 274 true $g(t)$, and thus we consider our modeled estimates of $g(t)$ to be first-order approximations. Analyzing a greater range of
 275 samples with a greater number of $\pm\text{CA}$ *in-situ* U–Pb analyses, with ideal datasets having 100s or even 1000s of analyses per
 276 sample (e.g., Pullen et al., 2014; Sundell et al., 2021), would likely improve our ability to constrain the form(s) of $g(t)$ and
 277 evaluate whether the logit-normal distribution or other forms of $g(t)$ are appropriate. Such datasets would also be more
 278 amenable to nonparametric solutions of estimating $g(t)$.

280 3. For $g(t)$ to represent the true distribution of Pb loss, the process of convolution must be applied to Pb^*/U ratios at the
 281 time of Pb loss. Because Pb^* is progressively added to the crystal over time, a greater amount of ancient Pb loss is required to
 282 achieve the same reduction in Pb^*/U relative to recent Pb loss. This point is illustrated in Figure 1 where a 50% reduction in
 283 Pb^* at 125 Myr after crystallization produces a similar reduction in $^{206}\text{Pb}^*/^{238}\text{U}$ when compared to zircon of the same age that
 284

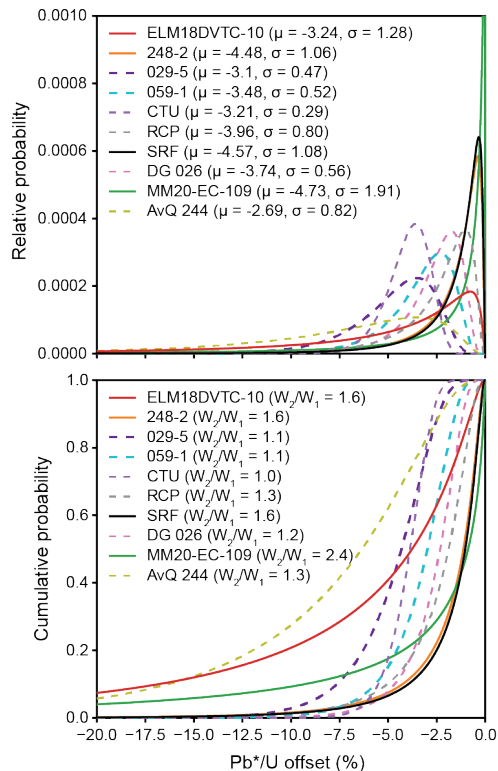


Figure 6. Distributions of apparent Pb loss when modeled as a logit-normal distribution. Samples with $\sigma < 1$ are shown as a dashed line.

285 lost 25% of its Pb* at 250 Myr (present day). For this reason, $g(t)$ can be viewed as a minimum estimate in the case of ancient
286 Pb loss. If the timing of Pb loss is known or can be estimated (e.g., Morris et al., 2015), the input Pb*/U ratios can be adjusted
287 prior to analysis such that $g(t)$ more accurately reflects the true magnitude of Pb loss.

288

289 4. The modeling framework presented above is designed for a group of cogenetic crystals with a shared crystallization
290 age (e.g., autocrystic zircon from the same magmatic episode; Miller et al., 2007). This requirement stems from our definition
291 of apparent Pb loss as a relative shift, or percentage deviation from the true isotopic value (Fig. 2). The assumption that all
292 zircon are coeval is a simplification, as even autocrystic zircon crystallize over a period of time, typically 10^3 - 10^4 yr timescales
293 (Miller et al., 2007; Rossignol et al., 2019). Multimodal detrital samples or igneous samples with xenocrystic or inherited
294 zircon are not easily modeled because these samples would violate our assumption of a shared crystallization age. Failure to
295 recognize the true heterogeneity in crystallization age in such a sample could cause an incorrect interpretation of the apparent
296 Pb loss distribution.

297

298 5. For datasets with paired non-CA and CA measurements, our modeling approach assumes that the relative precision
299 of the analyses is similar. This is because the Gaussian distribution that best approximates the CA U–Pb date distribution, $f(t)$,
300 is convolved with the apparent Pb loss distribution $g(t)$ to fit the non-CA U–Pb date distribution. The Watts et al. (2016) SIMS
301 dataset shows similar relative precision regardless of treatment approach (non-CA versus CA). Some samples from the von
302 Quadt et al. (2014) LA-ICP-MS dataset exhibit slightly lower relative precisions for non-CA versus CA, with sample AvQ
303 244 yielding the largest difference with an average relative precision of 1.1% (1σ) for non-CA dates and 0.8% (1σ) for CA
304 dates. We suggest that for the purposes of modeling apparent Pb loss, paired non-CA and CA U–Pb datasets should be collected
305 on the same instrument using similar acquisition parameters to avoid introducing large changes in measurement precision.
306 Alternatively, the CA U–Pb dates may be used to only constrain the μ of $f(t)$ in the model, with σ treated as an unknown
307 parameter (e.g., for paired non-CA LA-ICP-MS and CA-ID-TIMS datasets; Figs. 5a and 5i).

308

309 6. For datasets with paired non-CA and CA measurements, we do not consider any imperfections of the chemical
310 abrasion process. For example, although the CA treatment aims to completely remove all radiation damaged zones of the
311 crystal (Mattinson, 2005), it is possible to have remaining residual zones of Pb loss following treatment (e.g., Schoene et al.,
312 2010). Any such remaining compromised domains of the crystal will yield at least some apparent Pb loss when analyzed. For
313 instance, Watts et al. (2016) interpreted three zircon U–Pb analyses from SRF to have some residual Pb loss that was not fully
314 accounted for by the CA process (Fig. 5g). Incorporation of Pb loss-perturbed U–Pb dates when modeling $f(t)$ would likely
315 produce an underestimate of the true magnitude of the apparent Pb loss.

316

317

318

319 5.2 Distributions of apparent Pb loss

320 What distribution type(s) characterize apparent Pb loss in natural samples? Our results strongly suggest that at least nine of the
321 10 samples modeled have at least some systematic negative offset in $^{206}\text{Pb}^*/^{238}\text{U}$ that cannot be explained by random
322 measurement uncertainties alone. This is because the K-S and Kuiper statistical tests are unable to reject the null hypothesis
323 for many of the apparent Pb loss distribution types considered (Table A1). For example, only the no Pb loss scenario produced
324 a p -value < 0.05 for sample MM20-EC-109, suggesting that any of the other modeled distributions of apparent Pb loss may be
325 statistically plausible for this sample. These results suggest that we cannot confidently distinguish between discrete (constant
326 or isolated) or continuous distributions of apparent Pb loss in the datasets modeled. Except for ELM18DVTC-10 which has
327 144 non-CA LA-ICP-MS analyses, the samples we analyzed have relatively low numbers of analyses (between 17 and 68,
328 average of 32) for a given sample and treatment category (non-CA or CA) (Table 1). We suspect that collection of larger- n
329 datasets would allow better resolution of which parameterizations of $g(t)$ might be most appropriate.

330

331 Even if the specific distribution type(s) that characterizes $g(t)$ cannot be uniquely identified, our analysis suggests two
332 contrasting behaviors in apparent Pb loss (Fig. 6). We speculate that U–Pb dates that undergo a bulk shift (i.e., $W_2/W_1 \cong 1$)
333 may reflect a population of zircon crystals with relatively homogenous characteristics (e.g., size, U content, etc.) that have all
334 experienced a similar post-crystallization history. Correspondingly, the population of zircon that produces U–Pb dates with a
335 highly asymmetric distribution of age offset (i.e., $W_2/W_1 > \sim 1.5$) may reflect heterogeneity between crystals, with variable
336 characteristics. For example, Pb loss is thought to be promoted in small zircon crystals and in zircon with elevated U (Ashwal
337 et al., 1999; Gehrels et al., 2020), and thus distributions of particle size and/or trace element geochemistry may influence
338 asymmetric patterns in $g(t)$. Collection of size measurements and trace element concentrations from zircon in addition to
339 measurement of the U–Pb date (e.g., Watts et al., 2016) would likely help evaluate hypotheses about the underlying factors
340 that influence apparent Pb loss distributions. Furthermore, given the relatively small number of samples modeled in this study,
341 we suggest that there is a need for more samples to undergo paired non-CA and CA characterization to improve understanding
342 of the range of behaviors that may be typical. For example, it is presently unclear whether it is more common for samples to
343 have their U–Pb dates bulk shifted (e.g., samples 029-5, 059-1, CTU, DG 026) versus having relatively few U–Pb dates highly
344 offset (e.g., samples MM20-EC-109 and ELM18DVTC-10; Fig. 5).

345

346 Why do some samples experience more overall apparent Pb loss than others? Although we anticipated that apparent Pb loss
347 would be greater for samples with greater radiation damage due to U and Th decay, our analysis shows no clear trend by alpha
348 dose (Table 1). However, we acknowledge that the relatively high degree of apparent Pb loss modeled in the youngest sample,
349 ELM18DVTC-10, may be a consequence of contamination from overlying units, instead of true Pb loss (Miller et al., 2022).
350 Even the three samples from the same Eocene caldera system (CTU, RCP, and SRF) showed contrasting amounts of apparent

351 Pb loss (W_2 ranges from 2.9 to 4.2; Table 1) as noted by Watts et al. (2016). Characterizing the overall magnitude of apparent
352 Pb loss in a wider range of samples would likely help elucidate predictive factors, if any.

353

354 **5.3 Importance of quantifying the distribution of apparent Pb loss in *in-situ* U–Pb geochronology**

355 The overwhelming majority of published *in-situ* U–Pb dates from zircon, minimally >600,000 and likely in the millions of
356 analyses (Puetz et al., 2021), have not been treated using CA. In contrast, CA is now practiced routinely in the ID-TIMS
357 community which has contributed to growing precision and accuracy over the past two decades (Schoene, 2013). However,
358 the strategy of mitigating Pb loss through avoidance is perhaps less easily adopted to routine *in-situ* U–Pb geochronology. For
359 instance, there may be practical limitations with chemically abrading large numbers of zircon crystals, including the potential
360 loss of certain age modes that would be detrimental to provenance analysis. We thus suggest that there is a pressing need to
361 improve quantitative characterization of apparent Pb loss distributions in non-CA *in-situ* U–Pb datasets to aid in interpreting
362 these datasets and to guide strategies for future data collection.

363

364 It is somewhat concerning that nine of the 10 samples analyzed in this study exhibited statistically significant amounts of
365 negative age offset from the estimated true crystallization age. Even a small age offset of a few percent, or cryptic Pb loss
366 (Kryza et al., 2012; Watts et al., 2016), has potentially important repercussions for interpreting the age and rates of geologic
367 events and processes. For example, there is a growing awareness in the detrital geochronological community that the youngest
368 zircon U–Pb dates often skew unexpectedly young relative to the plausible crystallization age (e.g., Herriot et al., 2019; Gehrels
369 et al., 2020; Schwartz et al., 2022). Presently, there is no consensus on the importance of post-depositional Pb loss on
370 influencing depositional age interpretations (e.g., Herriott et al., 2019; Copeland, 2020; Schwartz et al., 2022). Sample MM20-
371 EC-109 illustrates the risk well; we initially interpreted the young tail on the U–Pb date distribution to suggest a depositional
372 age of ~125 Ma based on the youngest cluster of overlapping U–Pb dates. The youngest single analysis was a 60.5 ± 2.4 Ma
373 rim on a 135.3 ± 3.0 Ma core, with the second youngest being a 79 ± 1.2 Ma date measured from the core of a zircon crystal,
374 with the corresponding rim yielding an older 129.8 ± 3.6 Ma date (Table A2). Interpretation of the youngest single U–Pb date
375 or dates as the depositional age of this sample would have produced a highly erroneous estimate, off by up to -58% of the true
376 eruption age of 144.50 ± 0.07 (2σ) Ma as determined by CA-ID-TIMS. Because this ash is interbedded within a sequence of
377 organic rich marine mudstone in the Austral Basin of Argentina, the misinterpretation in this case could have led to an
378 erroneous depositional age model with implications for interpreting the paleoclimatic and geodynamic context of these
379 sediments.

380

381 Although modeling detrital samples was outside of the scope of this study, we believe that our results bear upon maximum
382 depositional age analysis. The tendency for the youngest U–Pb dates in a sample to be affected by Pb loss (or other similar

383 process) complicates even conservative estimates of the maximum depositional age (Dickinson and Gehrels., 2009; Coutts et
384 al., 2019; Schwartz et al., 2022). If apparent Pb loss follows a continuous distribution (e.g., Fig. 3d), then it is ill-advised to
385 assume that outlying U–Pb dates may be rejected while the rest are considered unperturbed (see also discussion in Copeland,
386 2020). Even an interpretation based on the peak age probability of the youngest age mode is likely to be too young, because
387 the process of convolution produces a young shift in the mode of the distribution, in addition to creating a young tail (Fig. 3d;
388 Fig. A1). Because existing methods of calculating the maximum depositional age (Dickinson and Gehrels, 2009; Coutts et al.,
389 2019; Vermeesch, 2021) do not account for systematic negative age offsets, our analysis suggests that there is a higher
390 probability for erroneous estimates of the maximum depositional age if (1) there are a large number of zircon crystals with
391 crystallization ages that are close to the age of deposition, (2) the overall number of measured U–Pb analyses is very high,
392 and/or (3) the magnitude of apparent Pb loss is high. In addition, a heavy-tailed distribution of apparent Pb loss (i.e., W_2/W_1
393 $\gg 1$) will result in a greater probability of finding extremely offset Pb^*/U values.

394

395 **6 Conclusions**

396 This study presents a mathematical framework for quantifying the distribution of apparent Pb loss on U–Pb date distributions,
397 which could include true loss of radiogenic Pb or other processes that also produce a systematically negative age offset. We
398 show that a Pb loss-perturbed U–Pb date distribution from a set of zircon crystals with a shared crystallization age can be
399 represented by the convolution of a Gaussian distribution that reflects measurement uncertainty in Pb^*/U with a distribution
400 that characterizes Pb loss, $g(t)$. Our approach relies on analyzing differences between the untreated Pb^*/U distribution from
401 *in-situ* U–Pb geochronology (i.e., LA-ICP-MS or SIMS) and an independent estimate of the true crystallization age, which
402 could include U–Pb dates from a thermally annealed and chemically abraded aliquot of the same sample or from another
403 geochronometer (e.g., $^{40}Ar/^{39}Ar$). We suggest that the first and second Wasserstein distances (W_1 and W_2) of the apparent Pb
404 loss distribution can be used to quantify the total degree of apparent Pb loss that a set of zircon analyses has undergone, with
405 maximum possible W_1 and W_2 values of 100.

406

407 We apply this modeling framework to ten igneous samples (Miocene to Carboniferous) analyzed with LA-ICP-MS or SIMS.
408 All but one of the samples showed a high probability that the untreated U–Pb date distribution has been perturbed by Pb loss
409 or other equivalent process. Although our analysis shows that multiple parameterizations of $g(t)$ can achieve statistically
410 acceptable fits (i.e., K-S or Kuiper p -value >0.05), we suggest that the logit-normal distribution may be a reasonable choice
411 for exploratory modeling of apparent Pb loss distributions. However, we caution that the number of analyses in the samples
412 we analyzed was generally low (17-144, average of 39); future efforts to characterize $g(t)$ may be promoted by collection of
413 larger- n datasets and through development of nonparametric methods of estimating $g(t)$. Furthermore, our estimates of $g(t)$
414 should be viewed as minimum estimates of the true amount of Pb lost, as we assumed present-day Pb loss in our analysis.

415 These caveats aside, we noted two behaviors of apparent Pb loss; samples with a bulk shift in U–Pb date distributions (W_2/W_1
416 $\lesssim 1.3$) and samples where most analyses had very little offset but fewer had much larger offsets ($W_2/W_1 \gtrsim 1.6$). The overall
417 magnitude of Pb^*/U decrease was also found to be variable, with median values varying from -0.9% to -6.4%.

418

419 Given the widespread application of *in-situ* U–Pb geochronology of untreated zircon across many disciplines of geosciences,
420 improved characterization of both the distribution type(s) and magnitude of apparent Pb loss is warranted, particularly for
421 Phanerozoic zircon where cryptic Pb loss is difficult to identify. We highlight a need for increased sampling and high- n
422 characterization of paired non-CA and CA *in-situ* U–Pb datasets. In addition, we recommend simultaneous collection of
423 parameters such as zircon size and trace elemental concentrations to aid in future efforts to understand the mechanisms of
424 negative age offsets. Ultimately, we anticipate that improved characterization of the magnitude of apparent Pb loss will aid in
425 interpreting non-CA *in-situ* U–Pb datasets and guide strategies for future data collection.

426 **Data availability**

427 Data are archived under <https://doi.org/10.5281/zenodo.8302521>. Appendix A provides a description of exploratory modeling
428 of different parameterizations of $g(t)$. Figure A1 includes examples of eight continuous distribution types not explored in the
429 main text. Table A1 and Figure A2 include summaries of all model results. Table A2 presents a summary of model fit for each
430 sample and distribution type considered. Tables A3 and A4 provide U–Pb analytical results for sample MM20-EC-109 from
431 the University of Arizona LaserChron Center (LA-ICP-MS) and Boise State University Isotope Geology Laboratory (CA-ID-
432 TIMS), respectively. Figure A3 includes CL images from the University of Arizona LaserChron Center. Supplemental Video
433 1 provides an example of convolution. Supplemental Video 2 presents an exploration of the parameter space for the logit-
434 normal distribution.

435

436 **Code availability**

437 Code used in this research is available on GitHub (https://github.com/grsharman/Pb_loss_modeling) with the v2.0.0 commit
438 archived under <https://doi.org/10.5281/zenodo.8302313>.

439

440 **Video supplement**

441 Supplemental Video 1 is available at <https://doi.org/10.5281/zenodo.8302521>. This animation provides an illustration of how
442 a Gaussian distribution of U–Pb dates (solid, blue line), $f(t)$, may be perturbed by logit-normal Pb loss, $g(t)$ (solid, red line).
443 The Pb loss distribution is first reflected about the y-axis and then iteratively shifted by small values of t , $g(t-\tau)$ (dashed, red
444 line). The convolution of $f(t)$ and $g(t)$ at any given value of t equals the summed area underneath the product of $f(t)$ and $g(t-\tau)$.
445 Supplemental Video 2 is also available at <https://doi.org/10.5281/zenodo.8302521> and illustrates how the logit-normal
446 distribution varies with respect to its two parameters μ and σ . Note that we have rescaled the x-axis of the logit-normal
447 distribution such that $-100 < x < 0$.

448

449 **Author contribution**

450 G. Sharman and M. Malkowski co-designed the study. G. Sharman developed the code. M. Malkowski produced the U–Pb
451 data from sample MM20-EC-109. G. Sharman and M. Malkowski wrote the manuscript.

452

453 **Competing interests**

454 The authors declare that they have no conflict of interest.

455

456 **Acknowledgments**

457 That authors thank Mark Pecha, George Gehrels, and staff at the University of Arizona LaserChron (supported by NSF-EAR
458 awards #1649254 and #2050246) as well as Jim Crowley and Mark Schmitz at the Isotope Geology Laboratory at Boise State
459 University. The project is supported in part by NSF EAR award #2243685, American Chemical Society Petroleum Research
460 Fund award #66408-DNI8, and the industrial affiliate members of the Detrital Geochronological Laboratory. We thank Kevin
461 Befus for coding advice. This work benefited from discussions with Alex Lipp and Greg Dumond. Comments and suggestions
462 from two anonymous reviewers and associate editor Pieter Vermeesch resulted in substantial improvements to the manuscript.

463 **References**

- 464 Aitchison, J., and Bacon-Shone, J.: Convex linear combinations of compositions, *Biometrika*, 86, 351-364,
465 <https://www.jstor.org/stable/2673517>, 1999.
- 466 Aitchison, J., and Shen, S. M.: Logistic-normal distributions: Some properties and uses, *Biometrika*, 67, 261-272,
467 <https://www.jstor.org/stable/2335470>, 1980.
- 468 Allen, C. M. and Campbell, I. H.: Identification and elimination of a matrix-induced systematic error in LA-ICP-MS
469 $^{206}\text{Pb}/^{238}\text{U}$ dating of zircon, *Chemical Geology*, 332, 157-165, 2012.
- 470 Anderson, T.: Correction of common lead in U-Pb analyses that do not report ^{204}Pb , *Chemical Geology*, 192, 59-79, 2002.
- 471 Andersen, T. and Elburg, M. A.: Open-system behaviour of detrital zircon during weathering: an example from the
472 Palaeoproterozoic Pretoria Group, South Africa, *Geological Magazine*, 159, 561-576, 2022.
- 473 Andersen, T., Elburg, M. A. and Magwaza, B. N.: Sources of bias in detrital zircon geochronology: Discordance, concealed
474 lead loss and common lead correction, *Earth-Science Reviews*, 197, 102899, 2019.
- 475 Ashwal, L. D., Tucker, R. D., and Zinner, E. K.: Slow cooling of deep crustal granulites and Pb-loss in zircon, *Geochimica et*
476 *Cosmochimica Acta*, 63, 2839-2851, 1999.
- 477 Balan, E., Neuville, D. R., Trocellier, P., Fritsch, E., Muller, J. P., and Calas, G.: Metamictization and chemical durability of
478 detrital zircon, *Am. Mineral.*, 86, 1025-1033, 2001.
- 479 Black, L. P.: Recent Pb loss in zircon: A natural or laboratory induced phenomenon?, *Chem. Geol. Isotope Geoscience section*,
480 65, 25-33, 1987.
- 481 Blackburn, T., Bowring, S. A., Schoene, B., Mahan, K., and Dudas, F.: U-Pb thermochronology: creating a temporal record
482 of lithosphere thermal evolution, *Contrib. Mineral. Petrol.*, 162, 479-500, [https://doi.org/10.1007/s00410-011-](https://doi.org/10.1007/s00410-011-0607-6)
483 [0607-6](https://doi.org/10.1007/s00410-011-0607-6), 2011.
- 484 Bowring, S. A. and Schmitz, M. D.: High-precision U-Pb zircon geochronology and the stratigraphic record, *Rev. Mineral.*
485 *Geochemistry*, 53, 305-326, 2003.
- 486 Burgess, S. D., Bowring, S., and Shen, S. Z.: High-precision timeline for Earth's most severe extinction, *Proc. Natl. Acad. Sci.*
487 *U. S. A.*, 111, 3316-3321, 2014.
- 488 Cherniak, D. J. and Watson, E. B.: Pb diffusion in zircon, *Chem. Geol.*, 172, 5-24, 2001.
- 489 Copeland, P.: On the use of geochronology of detrital grains in determining the time of deposition of clastic sedimentary strata,
490 *Basin Research*, 32, 1532-1546, 2020.
- 491 Compston, W.: Interpretations of SHRIMP and isotope dilution zircon ages for the geological time-scale: I. The early
492 Ordovician and late Cambrian, *Mineral. Mag.*, 64, 43-57, 2000a.
- 493 Compston, W.: Interpretation of SHRIMP and isotope dilution zircon ages for the Palaeozoic time-scale: II. Silurian to
494 Devonian, *Mineral. Mag.*, 64, 1127-1171, 2000b.

495 Coutts, D. S., Matthews, W. A., and Hubbard, S. M.: Assessment of widely used methods to derive depositional ages from
496 detrital zircon populations, *Geosci. Front.*, 34, 1421-1435, 2019.

497 Crowley, Q. G., Heron, K., Riggs, N., Kamber, B., Chew, D., McConnell, B., and Benn, K.: Chemical abrasion applied to LA-
498 ICP-MS U–Pb zircon geochronology, 4, 503–518, 2014.

499 Davis, D.W., Williams, I.S., and Krogh, T.E.: Historical development of zircon geochronology, *Reviews in Mineralogy and*
500 *Geochemistry*, 53, 145-181, <https://doi.org/10.2113/0530145>, 2003.

501 Dickinson, W. R. and Gehrels, G. E.: Use of U–Pb ages of detrital zircons to infer maximum depositional ages of strata: A test
502 against a Colorado Plateau Mesozoic database, *Earth Planet. Sci. Lett.*, 288, 115–125, 2009.

503 Froude, D. O., Ireland, T. R., Kinny, P. D., Williams, I. S., Compston, W., Williams, I. R., and Myers, J. S.: Ion microprobe
504 identification of 4,100–4,200 Myr-old terrestrial zircons, *Nature*, 304, 616, 1983.

505 Geisler, T., Pidgeon, R. T., Van Bronswijk, W., and Kurtz, R.: Transport of uranium, thorium, and lead in metamict zircon
506 under low-temperature hydrothermal conditions, *Chem. Geol.*, 191, 141–154, 2002.

507 Geisler, T., Pidgeon, R. T., Kurtz, R., van Bronswijk, W., and Schleicher, H.: Experimental hydrothermal alteration of partially
508 metamict zircon, *Am. Mineral.*, 88, 1496–1513, 2003.

509 Gehrels, G. E.: Detrital Zircon U–Pb Geochronology Applied to Tectonics, *Annu. Rev. Earth Planet. Sci.*, 42, 127–149, 2014.

510 Gehrels, G., Giesler, D., Olsen, P., Kent, D., Marsh, A., Parker, W., Rasmussen, C., Mundil, R., Irmis, R., Geissman, J., and
511 Lepre, C.: LA-ICPMS U–Pb geochronology of detrital zircon grains from the Coconino, Moenkopi, and Chinle
512 formations in the Petrified Forest National Park (Arizona), 2, 257–282, 2020.

513 Gradstein, F. M., Ogg, J. G., Smith, A. G., Bleeker, W., and Lourens, L. J.: A new Geologic Time Scale, with special reference
514 to Precambrian and Neogene, *Episodes*, 27, 83–100, 2004.

515 Grushka, E.: Characterization of Exponentially Modified Gaussian Peaks in Chromatography, *Anal. Chem.*, 44, 1733–1738,
516 1972.

517 Herriott, T. M., Crowley, J. L., Schmitz, M. D., Wartes, M. A., and Gillis, R. J.: Exploring the law of detrital zircon: LA-ICP-
518 MS and CA-TIMS geochronology of Jurassic forearc strata, Cook Inlet, Alaska, USA, 47, 1044-1048, 2019.

519 Howard, B., Sharman, G., Crowley, J. L., and Wersan, E. R.: The instrumentation dilemma: A comparison of paired LA-ICP-
520 MS and ID-TIMS U–Pb dates from zircon, *Geological Society of America Abstracts with Programs*, 54, 2022.

521 Ireland, T. R. and Williams, I. S.: Considerations in zircon geochronology by SIMS, *Rev. Mineral. Geochemistry*, 53, 215–
522 241, 2003.

523 Johnstone, S. A., Schwartz, T. M., and Holm-Denoma, C. S.: A Stratigraphic Approach to Inferring Depositional Ages From
524 Detrital Geochronology Data, 7, article 57, 2019.

525 Kaufmann, B.: Calibrating the Devonian Time Scale: A synthesis of U–Pb ID-TIMS ages and conodont stratigraphy, *Earth-*
526 *Science Rev.*, 76, 175–190, 2006.

527 Kirkland, C. L., Abello, F., Danišik, M., Gardiner, N.J., and Spencer, C.: Mapping temporal and spatial patterns of zircon U–
528 Pb disturbance: A Yilgarn Craton case study, *Gondwana Research*, 52, 39-47,
529 <https://dx.doi.org/10.1016/j.gr.2017.08.004>, 2017.

530 Kirland, C. L., Barnham, M., and Danišik, M.: Find a match with triple-dating: Antarctic sub-ice zircon detritus on the modern
531 shore of Western Australia, *Earth and Planetary Science Letters*, 531, 115953,
532 <https://doi.org/10.1016/j.epsl.2019.115953>, 2020.

533 Kröner, A., Jaekel, P., and Williams, I. S.: Pb-loss patterns in zircons from a high-grade metamorphic terrain as revealed by
534 different dating methods: U–Pb and Pb–Pb ages for igneous and metamorphic zircons from northern Sri Lanka,
535 *Precambrian Res.*, 66, 151–181, 1994.

536 Kryza, R., Crowley, Q. G., Larionov, A., Pin, C., Oberc-Dziedzic, T., and Mochnacka, K.: Chemical abrasion applied to
537 SHRIMP zircon geochronology: An example from the Variscan Karkonosze Granite (Sudetes, SW Poland),
538 *Gondwana Res.*, 21, 757–767, 2012.

539 Lipp, A.G., and Vermeesch, P.: Short communication: The Wasserstein distance as a dissimilarity metric for comparing detrital
540 age spectra and other geological distributions, *Geochronology*, 5, 263-270, [https://doi.org/10.5194/gchron-5-263-](https://doi.org/10.5194/gchron-5-263-2023)
541 [2023](https://doi.org/10.5194/gchron-5-263-2023), 2023.

542 Marsellos, A. E. and Garver, J. I.: Radiation damage and uranium concentration in zircon as assessed by Raman spectroscopy
543 and neutron irradiation, *Am. Mineral.*, 95, 1192–1201, 2010.

- 544 Mattinson, J. M.: Zircon U–Pb chemical abrasion (“CA-TIMS”) method: Combined annealing and multi-step partial
545 dissolution analysis for improved precision and accuracy of zircon ages, *Chem. Geol.*, 220, 47–66, 2005.
- 546 Mead, R.: A generalized logit-normal distribution, *Biometrics*, 21, 721–732, <https://www.jstor.org/stable/2528553>,
547 1965.
- 548 Mezger, K. and Krogstad, J. E.: Interpretation of discordant U–Pb zircon ages: An evaluation, *J. Metamorph. Geol.*, 15, 127–
549 140, 1997.
- 550 Miller, J. S., Matzel, J. E. P., Miller, C. F., Burgess, S. D., and Miller, R. B.: Zircon growth and recycling during the assembly
551 of large, composite arc plutons, *J. Volcanol. Geotherm. Res.*, 167, 282–299, 2007.
- 552 Miller, E. L., Raftrey, M. E., and Lund Snee, J.-E.: Downhill from Austin and Ely to Las Vegas: U–Pb detrital zircon suites
553 from the Eocene–Oligocene Titus Canyon Formation and associated strata, Death Valley, California, *Geol. Soc. Am.*
554 *Spec. Pap.*, 555, 359–378, 2022.
- 555 Morris, G. A., Kirkland, C. L., and Pease, V.: Orogenic paleofluid flow recorded by discordant detrital zircons in the
556 Caledonian foreland basin of northern Greenland, 7, 138–143, 2015.
- 557 Nasdala, L., Hanchar, J. M., Kronz, A., and Whitehouse, M. J.: Long-term stability of alpha particle damage in natural zircon,
558 *Chem. Geol.*, 220, 83–103, 2005.
- 559 Orejana, D., Merino Martínez, E., Villaseca, C., and Andersen, T.: Ediacaran–Cambrian paleogeography and geodynamic
560 setting of the Central Iberian Zone: Constraints from coupled U–Pb–Hf isotopes of detrital zircons, *Precambrian Res.*,
561 261, 234–251, 2015.
- 562 Pidgeon, R. T., O’Neil, J. R., and Silver, L. T.: Uranium and lead isotopic stability in metamict zircon under experimental
563 hydrothermal conditions, *Science*, 154, 1538–1540, <https://www.jstor.org/stable/1720453>, 1966.
- 564 Pidgeon, R. T., Nemchin, A. A., and Whitehouse, M. J.: The effect of weathering on U–Th–Pb and oxygen isotope systems of
565 ancient zircons from the Jack Hills, Western Australia, *Geochim. Cosmochim. Acta*, 197, 142–166, 2017.
- 566 Pidgeon, R. T., Nemchin, A. A., Roberts, M. P., Whitehouse, M. J., and Bellucci, J. J.: The accumulation of non-formula
567 elements in zircons during weathering: Ancient zircons from the Jack Hills, Western Australia, *Chem. Geol.*, 530,
568 119310, <https://doi.org/10.1016/j.chemgeo.2019.119310>, 2019.
- 569 Press, W. H., Teukolsky, S. A., Vetterling, W. T., and Flannery, B. P.: *Numerical Recipes: The Art of Scientific Computing*,
570 3rd Editio., Cambridge University Press, 1235 pp., 2007.
- 571 Puetz, S. J., Spencer, C. J., and Ganade, C. E.: Analyses from a validated global U–Pb detrital zircon database: Enhanced
572 methods for filtering discordant U–Pb zircon analyses and optimizing crystallization age estimates, *Earth-Science*
573 *Rev.*, 220, 103745, <https://doi.org/10.1016/j.earscirev.2021.103745>, 2021.
- 574 Pullen, A., Ibáñez-Mejía, M., Gehrels, G. E., Ibáñez-Mejía, J. C., and Pecha, M.: What happens when $n=1000$? Creating large-
575 n geochronological datasets with LA-ICP-MS for geologic investigations, *J. Anal. At. Spectrom.*, 29, 971–980, 2014.
- 576 Reimink, J. R., Davies, J. H. F. L., Waldron, J. W. F., and Rojas, X.: Dealing with discordance: A novel approach for analysing
577 U–Pb detrital zircon datasets, *J. Geol. Soc. London.*, 173, 577–585, 2016.
- 578 Rioux, M., Bowring, S., Kelemen, P., Gordon, S., Dudás, F., and Miller, R.: Rapid crustal accretion and magma assimilation
579 in the Oman–U.A.E. ophiolite: High precision U–Pb zircon geochronology of the gabbroic crust, *J. Geophys. Res.*
580 *Solid Earth*, 117, 2012.
- 581 Rossignol, C., Hallot, E., Bourquin, S., Pujol, M., Jolivet, M., Pellenard, P., Ducassou, C., Nalpas, T., Heilbronn, G., Yu, J.,
582 and Dabard, M. P.: Using volcanoclastic rocks to constrain sedimentation ages: To what extent are volcanism and
583 sedimentation synchronous?, *Sediment. Geol.*, 381, 46–64, 2019.
- 584 Ruiz, M., Schaltegger, U., Gaynor, S. P., Chiaradia, M., Abrecht, J., Gislser, C., Giovanoli, F., and Wiederkehr, M.: Reassessing
585 the intrusive tempo and magma genesis of the late Variscan Aar batholith: U–Pb geochronology, trace element and
586 initial Hf isotope composition of zircon, *Swiss J. Geosci.*, 115, 1–24, 2022.
- 587 Saylor, J. E. and Sundell, K. E.: Quantifying comparison of large detrital geochronology data sets, 12, 203–220,
588 <https://doi.org/10.1130/GES01237.1>, 2016.
- 589 Schoene, B., Guex, J., Bartolini, A., Schaltegger, U., and Blackburn, T. J.: Correlating the end-Triassic mass extinction and
590 flood basalt volcanism at the 100 ka level, *Geology*, 38, 387–390, <https://doi.org/10.1130/G30683.1>, 2010.
- 591 Schoene, B.: U–Th–Pb Geochronology, *Treatise on Geochemistry (Second Edition)*, 4, 341–378, 2013.

592 Schwartz, T. M., Souders, A. K., Lundstern, J.-E., Gilmer, A. K., and Thompson, R. A.: Revised age and regional correlations
593 of Cenozoic strata on Bat Mountain, Death Valley region, California, USA, from zircon U–Pb geochronology of
594 sandstones and ash-fall tuffs, *Geosphere*, 19, 235–257, 2022.

595 Sharman, G. R., Covault, J. A., Flaig, P. P., Dunn, R., Fussee-Durham, P., Larson, T. E., Shanahan, T. M., Dubois, K., Shaw,
596 J. B., Crowley, J. L., Shaulis, B.: Coastal response to global warming during the Paleocene-Eocene Thermal Maximum,
597 625, 111664, <https://doi.org/10.1016/j.palaeo.2023.111664>, 2023.

598 Silver, L. T. and Deutsch, S.: Uranium-Lead Isotopic Variations in Zircons: A Case Study, *J. Geol.*, 71, 721–758, 1963.

599 Snow, J. K. and Lux, D. R.: Tectono-sequence stratigraphy of Tertiary rocks in the Cottonwood Mountains and northern Death
600 Valley area, California and Nevada, *Geol. Soc. Am. Spec. Pap.*, 333, 17–64, 1999.

601 Solari, L. A., Ortega-Obregón, C., and Bernal, J. P.: U–Pb zircon geochronology by LAICPMS combined with thermal
602 annealing: Achievements in precision and accuracy on dating standard and unknown samples, *Chem. Geol.*, 414,
603 2015.

604 Spencer, C. J., Kirkland, C. L., and Taylor, R. J. M.: Strategies towards statistically robust interpretations of in situ U–Pb
605 zircon geochronology, *Geosci. Front.*, 7, 581–589, 2016.

606 Stern, T. W., Goldich, S. S., and Newell, M. F.: Effects of weathering on the U–Pb ages of zircon from the Morton Gneiss,
607 Minnesota, *Earth Planet. Sci. Lett.*, 1, 369–371, 1966.

608 Sundell, K. E., Gehrels, G. E., and Pecha, M. E.: Rapid U–Pb Geochronology by Laser Ablation Multi-Collector ICP-MS,
609 *Geostand. Geoanalytical Res.*, 45, 37–57, 2021.

610 Tilton, G. R., Patterson, C., Brown, H., Ingham, M., Hayden, R., Hess, D., and Larsen, E., J.: Isotopic composition and
611 distribution of lead, uranium, and thorium in a Precambrian granite, *Bull. Geol. Soc. Am.*, 66, 1131–1148, 1955.

612 Ver Hoeve, T. J., Scoates, J. S., Wall, C. J., Weis, D., and Amini, M.: Evaluating downhole fractionation corrections in LA-
613 ICP-MS U–Pb zircon geochronology, *Chem. Geol.*, 483, 201–217, 2018.

614 Vermeesch, P.: Dissimilarity measures in detrital geochronology, *Earth-Science Rev.*, 178, 310–321, 2018a.

615 Vermeesch, P.: Statistical models for point-counting data, *Earth-Science Rev.*, 501, 112–118, 2018b.

616 Vermeesch, P.: Maximum depositional age estimation revisited, *Geosci. Front.*, 12, 843–850, 2021.

617 von Quadt, A., Gallhofer, D., Guillong, M., Peytcheva, I., Waelle, M., and Sakata, S.: U–Pb dating of CA/non-CA treated
618 zircons obtained by LA-ICP-MS and CA-TIMS techniques: Impact for their geological interpretation, *J. Anal. At.*
619 *Spectrom.*, 29, 1618–1629, 2014.

620 Watts, K. E., Coble, M. A., Vazquez, J. A., Henry, C. D., Colgan, J. P. and John, D. A.: Chemical abrasion-SIMS (CA-SIMS)
621 U–Pb dating of zircon from the late Eocene Caetano caldera, Nevada *Chemical Geology*, 439, 139–151, 2016.

622 Wetherill, G. W.: Discordant Uranium-Lead Ages, 1, *Trans. Am. Geophys. Union*, 37, 320–326, 1956.

623 Willner, A. P., Sindern, S., Metzger, R., Ermolaeva, T., Kramm, U., Puchkov, V., and Kronz, A.: Typology and single grain
624 U/Pb ages of detrital zircons from Proterozoic sandstones in the SW Urals (Russia): Early time marks at the eastern
625 margin of Baltica, *Precambrian Res.*, 124, 1–20, 2003.

626 Zeh, A., Wilson, A. H., and Ovtcharova, M.: Source and age of upper Transvaal Supergroup, South Africa: Age-Hf isotope
627 record of zircons in Magaliesberg quartzite and Dullstroom lava, and implications for Paleoproterozoic (2.5–2.0 Ga)
628 continent reconstruction, *Precambrian Res.*, 278, 1–21, 2016.